Hindawi
Advances in Condensed Matter Physics
Volume 2019, Article ID 3176148, 12 pages
https://doi.org/10.1155/2019/3176148

Research Article

Structural, Electronic, Lattice Dynamic, and Elastic Properties of $SnTiO_3$ and $PbTiO_3$ Using Density Functional Theory

Shiferaw Kuma [1] **and Menberu Mengesha Woldemariam** [2]

[1]*Department of Physics, Wollega University, P.O. Box 395, Nekemte, Ethiopia*
[2]*Department of Physics, Jimma University, P.O. Box 378, Jimma, Ethiopia*

Correspondence should be addressed to Shiferaw Kuma; shifgadisa@gmail.com and Menberu Mengesha Woldemariam; menberu.mengesha@ju.edu.et

Received 18 March 2019; Revised 5 August 2019; Accepted 27 August 2019; Published 29 September 2019

Academic Editor: Sergio E. Ulloa

The structural, electronic, and elastic properties of tetragonal phase of $SnTiO_3$ and $PbTiO_3$ are investigated using first principle calculations. The unknown exchange-correlation functional is approximated with generalized gradient approximation (GGA) as implemented in pseudopotential plane wave approach. The convergence test of total energy with respect to energy cutoff and k-point sampling is preformed to ensure the accuracy of the calculations. The structural properties such as equilibrium lattice constant, equilibrium unit cell volume, bulk modulus, and its derivative are in reasonable agreement with the previous experimental and theoretical works. From elastic constants, mechanical parameters such as anisotropy factor A, shear modulus G, bulk modulus B, Young's modulus E, and Poison's ratio n are determined by using Voigt–Reuss–Hill average approximation. In addition, Debye temperature and longitudinal and transversal sound velocities are predicted from elastic constants. The electronic band structure and density of states of both compounds are obtained and compared with the available experimental as well as theoretical data. Born effective charge (BEC), phonon dispersion curve, and density of states are computed from functional perturbation theory (DFPT). Lastly, the spontaneous polarization is determined from the modern theory of polarization, and they are in agreement with the previous findings.

1. Introduction

ABO_3 perovskites are important for a variety of high technology applications as a result of their diverse physical properties [1]. Ferroelectric perovskite oxides are important for many emerging industrial applications including high capacity memory cells, catalysis, optical wave guides, integrated optics applications, and substrates for high-Tc cuprate superconductor growth [2]. Lead titanate ($PbTiO_3$) is one of the interesting and more studied perovskites possessing a ferroelectric phase under ambient conditions [3]. Due to its high spontaneous polarization and wide temperature stability of ferroelectric phase, the compound has got a strong interest. At room temperature, $PbTiO_3$ compound has a tetragonal phase (space group *P4mm*) with ferroelectric property, while for the temperature above 763 K, it shows cubic phase (space group *Pm3m*) with paraelectric characteristics [4]. For a long time, there have been some efforts towards determining the electronic and optical properties of the cubic and tetragonal state of $PbTiO_3$ from either first principles calculations or by experiment [5, 6]. But, from a theoretical point of view, a proper description of its electronic properties is still an area of active research. Theoretical computations have had difficulty in predicting the correct band gap energy and other related electronic properties of $PbTiO_3$ from first principle.

In spite of great physical importance, the most widely used ferroelectric ceramics based on the $PbTiO_3$ and $PbZrO_3$ solid solution are generically called PZT. The PZT is composed of about 60 percent of lead, which raises ecological concerns; thus, some countries have legislated to replace this

material by lead-free ceramics [7] since lead is a toxic element that affects the human health and the environment. As a result, recent studies have extensively focused on identifying new and more environmentally friendly ferroelectric materials and other alternative compounds [8]. The total replacement of Pb-based materials in technological devices remains almost improbable because of the unsatisfactory performance of other materials.

However, modification efforts to reduce the consumption of toxic Pb^{2+}, such as by substitution or doping techniques, remain necessary. $SnTiO_3$ is one of the promising Pb-free ferroelectric materials, which is theoretically having a high dielectric constant and ferroelectric polarization [9]. Recently, Sn^{2+} is widely used to design a novel piezoelectric of free Pb-based material using the first principle study. However, most of the theoretical reports with regard to the $SnTiO_3$ materials are merely focused on their physical properties and high polarization effect in the ferroelectric phase [10]. According to our knowledge, the elastic properties, Poison's ratio, anisotropic index, Debye temperature, born effective charge, phonon dispersion, and spontaneous polarization of tetragonal phase of $SnTiO_3$ which is, expected to replace $PbTiO_3$ is, not well studied and needs more investigation. In general, to predict a specific device application and improvements, a deeper and fundamental understanding of the properties of the ferroelectric material are necessary. Therefore, studying the structural, elastic, lattice dynamics, and electronic properties as well as understanding the overall characteristics of the system is utmost important.

2. Computational Method

Electronic and structural computations are performed by using density functional theory as implemented in the Quantum ESPRESSO (QE) open-source package. Plane wave self-consistent calculation (PWscf) is a first principle energy code that uses norm-conserving pseudopotentials (PP) and ultrasoft pseudopotentials (US-PP). It is well known that the exchange-correlation functional is the challenging term to approximate in first principle calculations. Today, the hybrid exchange functional like B3LYP and B3PW allows obtaining a band gap which is in good agreement with the experimental value [11, 12]. However, GGA-PBE [13] is used in this study to approximate the exchange-correlation functional as we have no pseudopotential generator for hybrid functional in Quantum ESPRESSO package currently. The k-point sampling of the Brillion zone is constructed using Monk Horst Pack Mesh scheme [14] with $6\times6\times6$ grids in primitive cells of compounds. The Born effective charges, optical dielectric constants, and phonon dispersion curve of the ferroelectric materials are calculated from density functional perturbation theory (DFPT) using local density approximation (LDA).

3. Results and Discussion

3.1. Total Energy with respect to Energy Cutoff and k-point Sampling. The convergence test for total minimum energy as a function of cutoff energy is performed with an increment of 10 Ry in the range of 20 to 130 Ry. While varying the energy cutoff, the other parameters in the input file are fixed. For good total minimum energy convergence, we have used the criteria that the change in energy (ΔE) from the minimum energy at the reference point (130 Ry) to be approximately equal to 4×10^{-4} Ry per atom. In our calculation, $\Delta E \cong 4.43\times10^{-4}$ per cell (8.86×10^{-5} Ry per atom) for $PbTiO_3$ at 80 Ry energy cutoffs and convergence is achieved. Moreover, $\Delta E \cong 4.13\times10^{-4}$ per cell (8.26×10^{-5} Ry per atom) for $SnTiO_3$ at 80 Ry energy cutoffs and the energy is converged. Similarly, the convergence test for total minimum energy versus k-point sampling with an increment of $2\times2\times2$ in the range from $2\times2\times2$ to $10\times10\times10$ is performed by fixing the other parameters constant. Based on the criteria, the convergence is achieved at $6\times6\times6$ k-point grid. The energy is monotonically decreasing with increasing cutoff energy due to a direct result of the variational principle. Moreover, it is possible to argue the energy is monotonically decreasing with respect to k-point grid size in this calculation. However, this does not necessarily happen all the time. The systematic trend cannot be predicted just by increasing the sampling point for the approximation to the integral Figure 1.

3.2. Structural Optimization and Bulk Modulus. To optimize the structural parameters of $SnTiO_3$ and $PbTiO_3$, 80 Ry cutoff energy and $6\times6\times6$ k-point grid size is used from our convergence test. For this calculation, we varied the value of lattice constant around the experimental value fixing other parameters. The lattice constant versus total minimum energy for both compounds is demonstrated in Figure 2. From this figure, one can see that the optimized equilibrium lattice constant of $SnTiO_3$ in tetragonal phase is $a = 3.89$ Å and $c = 4.130$ Å, which is in good agreement with other theoretical results [10]. Similarly, the calculated equilibrium lattice constant of $PbTiO_3$ is $a = 3.941$ Å and $c = 4.177$ Å, which is larger than the experimental value mentioned in [15, 16].

The calculation clearly shows that GGA overestimates the value of lattice constant. Moreover, fitting the calculated total energy at a number of lattice constant into the Murnaghan equation of state [17] is shown in Figure 3. The fitting helps to obtain the physical parameters such as bulk modulus, equilibrium unit cell volume, and the pressure derivatives of the bulk modulus.

Comparison of the calculated values of lattice constant, bulk modulus, equilibrium unit cell volume, and pressure derivatives of bulk modulus with experimental and previous theoretical results is shown in Table 1.

3.3. Elastic Properties. The elastic constants of solids are important parameters of a material and can provide valuable information about the mechanical stability, bonding character between adjacent atomic planes, brittleness, ductility, stiffness, and anisotropic character. The elastic constant tensors are determined from the

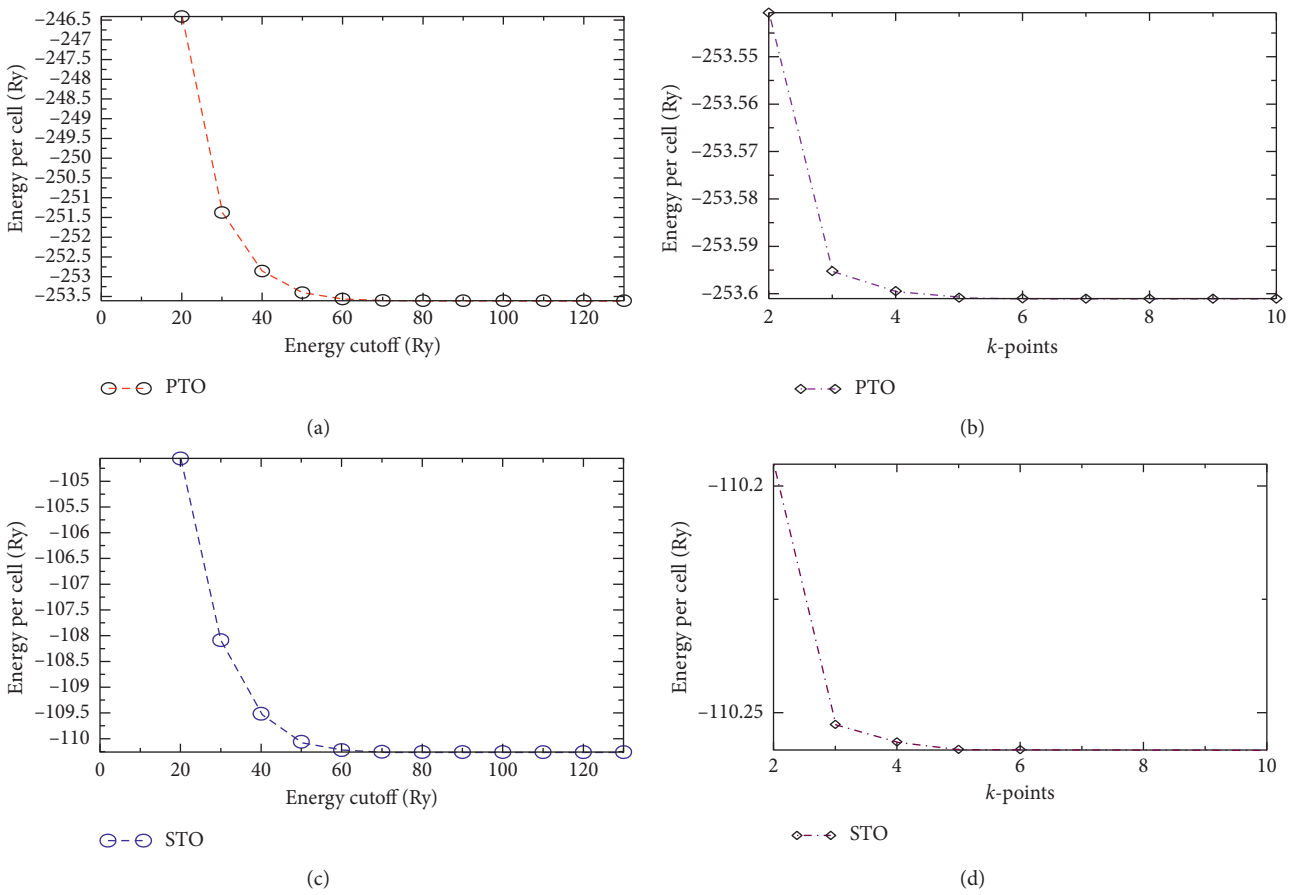

Figure 1: Convergence of absolute energies with respect to cutoff energies and k-point sampling for tetragonal phase of $SnTiO_3$ and $PbTiO_3$.

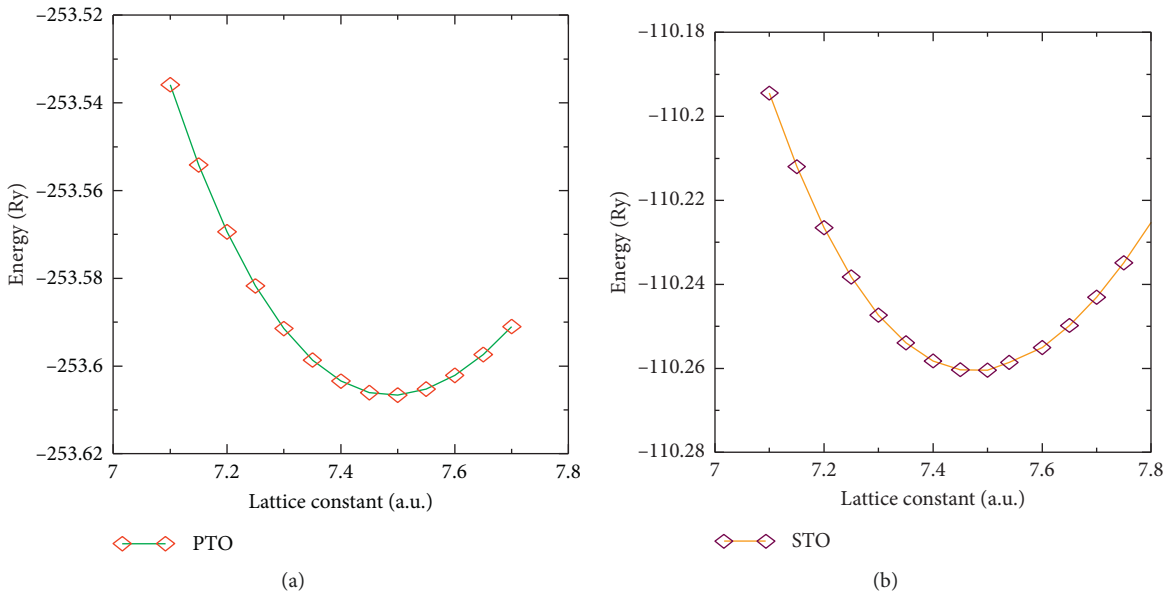

Figure 2: The lattice constant versus energy.

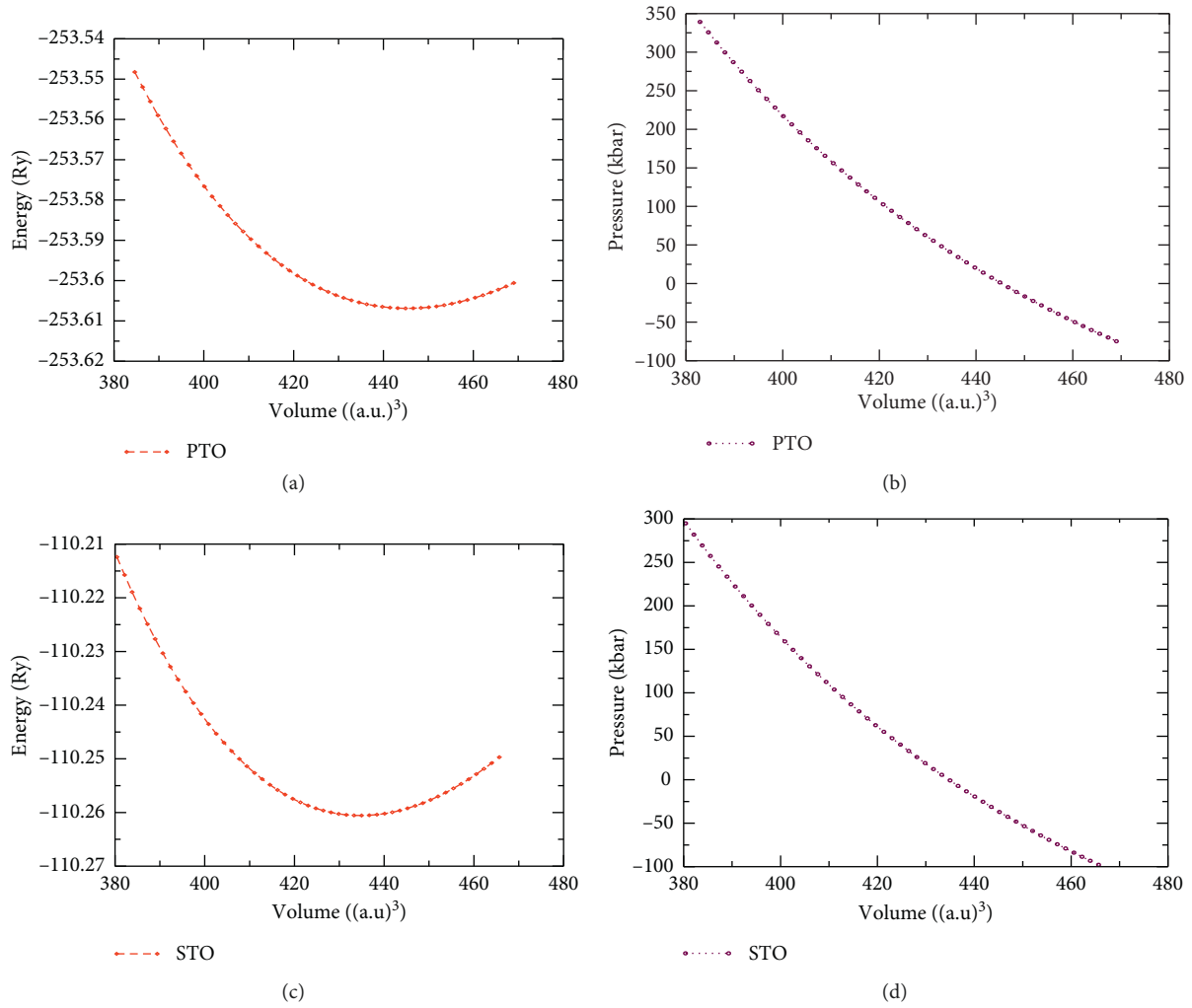

Figure 3: Variation of energy and pressure with respect to volume.

Table 1: Computed values of lattice constants, unit cell volume, and bulk modulus for both $SnTiO_3$ and $PbTiO_3$.

	$PbTiO_3$	$SnTiO_3$
Lattice constant (Å)	$a = 3.941$ and $c = 4.177$ Å (our calculation) $a = 3.904$ and $c = 4.152$ Å (expt.) [15, 16] $a = 3.81$ and $c = 4.6863$ Å (theory) [10]	$a = 3.895$ and $c = 4.130$ Å (our calculation) $a = 3.807$ and 4.538 Å (theory) [10]
Bulk modulus (GPa)	160.5	164.2
Unit cell volume (Å^3)	65.99 67.892 [16]	64.43 65.771 [10]
Bulk modulus derivative	4.24	4.23

knowledge of the derivative of energy as a function of lattice strain [18]:

$$C_{ijkl} = \left(\frac{\partial \sigma_{ij}}{\partial \varepsilon_{jkl}}\right)_x = \left(\frac{1}{V}\frac{\partial^2 E}{\partial \varepsilon_{ij}\varepsilon_{kl}}\right)_x. \quad (1)$$

In order to compute the elastic constants, we have used the method developed and maintained by Andrea Dal Corso as implemented in the QE package [19]. For tetragonal system, there are six independent elastic constants C_{11}, C_{12}, C_{13}, C_{33}, C_{44} and C_{66} that should satisfy Born's stability criteria [5]:

$$\begin{aligned} C_{11} - C_{12} &> 0, \\ C_{11} + C_{33} - 2C_{13} &> 0, \\ C_{11} &> 0, \\ C_{33} &> 0, \\ C_{44} &> 0, \\ C_{66} &> 0, \\ 2C_{11} + C_{33} + 2C_{12} + 4C_{13} &> 0, \\ \frac{1}{3}(C_{12} + 2C_{13}) < B &< \frac{1}{3}(C_{11} + 2C_{33}). \end{aligned} \tag{2}$$

The calculated elastic properties of $SnTiO_3$ and $PbTiO_3$ are compared to the available theoretical results in Table 2. From Table 2, we can see that Born's stability criteria given in equation (2) are well satisfied, which clearly indicates that both materials are mechanically stable. Using the Voigt–Reuss–Hill approximation, mechanical parameters such as bulk modulus B, sheared modulus G, Young's modulus E, and Poisson's ratio n are determined from the results of elastic constants. In the commonly used Voigt approximation [22],

$$\begin{aligned} B_V &= \frac{1}{9}[(C_{11} + C_{22} + C_{33}) + 2(C_{12} + C_{23} + C_{31})], \\ G_V &= \frac{1}{15}[(C_{11} + C_{22} + C_{33}) - (C_{12} + C_{23} + C_{31}) \\ &\quad + 3(C_{44} + C_{55} + C_{66})]. \end{aligned} \tag{3}$$

On the other hand, in Reuss approximation [23],

$$\begin{aligned} B_R &= [(S_{11} + S_{22} + S_{33}) + 2(S_{12} + S_{23} + S_{31})]^{-1}, \\ G_R &= 15[4(S_{11} + S_{22} + S_{33}) - (S_{12} + S_{13} + S_{23}) \\ &\quad + 3(S_{44} + S_{55} + S_{66})]^{-1}. \end{aligned} \tag{4}$$

Using energy considerations, Hill [24] proved that the Voigt and Reuss equations represent upper and lower limit as

$$\begin{aligned} G &= \frac{1}{2}(G_V + G_R), \\ B &= \frac{1}{2}(B_V + B_R). \end{aligned} \tag{5}$$

For all the averaged procedures presented, Young's modulus, E, and Poisson's ratio, n, can be obtained in connection with the bulk modulus, B, and the shear modulus, G, as

$$\begin{aligned} E &= \frac{9BG}{3B + G}, \\ n &= \frac{3B - 2G}{2(3B + G)}. \end{aligned} \tag{6}$$

The ratio of B/G helps to categorize the brittleness and ductility of different materials. According to Pugh [25], 1.75 is the critical value that separate the brittleness and ductility behaviors of materials. When the ratio of B/G is higher than the critical value, then the material is associated with ductility. However, when the ratio of B/G value is lower than the critical value, the material is considered as brittle. As indicated in Table 2, both compounds are categorized as ductile because the value of B/G is higher than the critical value. In addition, bulk modulus and shear modulus can be used to measure the material hardness. When the sheared modulus value increases, the material becomes stiffer. The results show that $PbTiO_3$ is stiffer than $SnTiO_3$.

The study of elastic anisotropy in material is of great significance to understand the mechanical properties of the crystal. The universal anisotropic index (A^U) is a measure to quantify the elastic anisotropic characteristics based on the contributions of both bulk and sheared modulus [26]:

$$A^U = \frac{5G_V}{G_R} + \frac{B_V}{B_R} - 6, \tag{7}$$

where G_V and B_V are shear and bulk modulus obtained from Voigt approximation, respectively. And similarly, G_R and B_R are shear and bulk modulus acquired from Reuss approximation. As it is described in (7), when the universal anisotropic index (A^U) is equal to zero, the crystal is an isotropic. The variation from zero defines the level of elastic anisotropic. Therefore, the obtained universal anisotropic index (A^U) is 0.18 for $PbTiO_3$ and 0.11 for $SnTiO_3$. The result reveals that comparatively small elastic anisotropic characteristics are observed in the tetragonal phase of materials. Poisson's ratio (n) is one of mechanical parameters which provides useful information about the characteristics of the bonding forces. In the evaluation of Poisson's ratio [27], 0.25 and 0.5 are the lower and upper limits of central force, respectively. The obtained values of Poisson's ratio for both materials in tetragonal phase are found between the lower and upper limits. This indicates that the interatomic forces of $PbTiO_3$ and $SnTiO_3$ are central. In the Debye model, once the elastic parameters are computed, the expression for Debye temperature at low temperature is given by [28, 29]

$$\theta = \frac{h}{k}\left[\frac{3n}{\pi}\left(\frac{N_A\rho}{M}\right)\right]^{1/3} v_m, \tag{8}$$

where h is Planck's constant, k is Boltzmann's constant, N_A is Avogadro's number, and v_m is the average sound velocity. The average sound velocity v_m is expressed in terms of longitudinal sound velocity v_l and transverse sound velocity v_t, which can be obtained from elastic constant parameters such as shear modulus (G) and the bulk modulus (B):

Table 2: Computed elastic properties of $SnTiO_3$ and $PbTiO_3$ as compared to the available theoretical results.

		C_{11}	C_{33}	C_{44}	C_{66}	C_{12}	C_{13}	B	G	B/G	N	E	A
$PbTiO_3$	Our work	313.1	197.0	82.72	85.41	110.71	92.40	152.67	84.3	1.80	0.26	213.7	0.18
	Expt.	235 [20]	105	65.1	104	101	99	104 [21]					
	Theory	280.5 [16]	279.7	98.6	98.6	118.5	118.5	172.4					
$SnTiO_3$	Our work	311.65	227.6	77.06	77.27	109.86	98.72	160.53	81.9	1.95	0.28	210.0	0.11

$$v_m = \left[\frac{1}{3}\left(\frac{2}{v_t^3} + \frac{1}{v_l^3}\right)\right]^{-1/3}, \quad (9)$$

$$v_l = \left(\frac{(B + (3/4G))}{\rho}\right)^{1/2}, \quad (10)$$

$$v_t = \left(\frac{G}{\rho}\right)^{1/2}. \quad (11)$$

The Debye temperature and longitudinal, transverse, and average sound velocities with respect to equations (8)–(11) are calculated, and the values are demonstrated in Table 3.

As it is shown in equation (8), the Debye temperature θ_D and average sound velocity v_m have direct relationship. For high value of the average sound velocity, the Debye temperature becomes higher. $SnTiO_3$ has high Debye temperature compared to $PbTiO_3$.

3.4. Electronic Band Structure and Density of States. The electronic band structures are plotted using GGA-PBE exchange-correlation functional along high symmetry axes of the Brillion zone as shown in Figure 4. From the calculations we obtained, the valance bands are separated from the conduction bands by an indirect band gap of 1.71 eV and 2.20 eV for $SnTiO_3$ and $PbTiO_3$, respectively. These values are smaller than the experimental values, but they are consistent with previous calculated values [30–32]. However, the difference between our computation and the experiment is attributed to insufficient precision to reproduce both exchange-correlation energy and its charge derivative.

In solid-state physics, the density of states (DOS) of a system describes the number of states per interval of energy at each energy level available to be occupied. The total density of states (TDOS) and partial density of states (PDOS) of $SnTiO_3$ and $PbTiO_3$ are shown in Figures 5 and 6. The highest valance bands is mainly dominated by 2p electron of O for all compositions of compounds, and the lowest conduction bands is mainly originated from the Ti-3d, Sn-5p, and Pb-6P states.

In order to know the chemical bonding and charge transfer in $PbTiO_3$ and $SnTiO_3$ perovskite compounds, the charge density behaviors in 2D are calculated in 100 and 110 planes as shown in Figures 7 and 8. According to the theory of Cohen [33], hybridization is important for forming soft mode leading to ferroelectric instability. The hybridization between the Ti-3d and O-2p orbitals in both compounds has strong hybridization.

3.5. Born Effective Charge (BEC) and Phonon Spectra. Born effective charges (BECs) of $PbTiO_3$ and $SnTiO_3$ were computed in the framework of DFPT using LDA exchange-correlation potential. The Born effective charges Z^* are tensors, defined as the first derivative of polarization with atomic displacement [34, 35]. Born effective charges play key role in understanding both the ferroelectric phase and lattice dynamics:

$$Z_{i\alpha\beta} = \frac{\Omega \partial P_\alpha}{e \partial u_{i\beta}}, \quad (12)$$

where α and β denote directions, P_α is the component of the polarization in the α^{th} direction, $u_{i\beta}$ is the periodic displacement of the i^{th} atom in the β^{th} direction, Ω is the unit cell volume, and e is the electron charge. The calculated born effective charge tensors of the atoms for both compounds are given in Tables 4 and 5.

As presented in Tables 4 and 5, the Born effective dynamical charge of Sn (4.21), Ti (7.57), and $O_{||}$ (−5.35) is larger than the nominal ionic charge. In the same way, the maximum dynamical charge of 3.83 for Pb, 7.77 for Ti and −5.12 for $O_{||}$ is larger than the purely ionic picture. Moreover, the large values of BEC of each atom compared to the nominal ionic charge show the importance of the ions as the driving force of the ferroelectric distortion. The computed values of dielectric constant of $SnTiO_3$ ($\varepsilon_{11} = \varepsilon_{22} = 9.81$ and $\varepsilon_{33} = 8.98$) are greater than those of $PbTiO_3$ ($\varepsilon_{11} = \varepsilon_{22} = 9.13$ and $\varepsilon_{33} = 8.21$).

In Figure 9, we plotted the phonon dispersion curves and vibrational density of state of $PbTiO_3$ and $SnTiO_3$ compounds along high symmetry directions in the first Brillouin zone. For our system, there are 15 vibrational modes.

The negative frequency in the plot shows the imaginary frequency in the dispersion below the zero frequency line is related to unstable modes. The behavior of phase transitions such as dielectric, ferroelectric, and piezoelectric can be determined from the zero line frequency which is named as unstable modes.

3.6. Spontaneous Polarization. Modern theory of polarization, namely, berry phase approach, is used to describe the ferroelectric materials theoretically. The spontaneous polarization (P) of the compounds is obtained from the sum of both ionic polarization (P_{ion}) and electronic polarization (P_{el}):

$$P_{ion} + P_{el} = \frac{|e|}{\Omega}\sum_k z_k u_k + \left(\frac{-2|e|i}{(2\pi)^3}\int_A dk \sum_1^M \int_0^G \left\langle u_{nk}\left|\frac{\partial}{\partial k}\right|u_{nk}\right\rangle\right), \quad (13)$$

Table 3: Calculated longitudinal, transverse, average sound velocity (v_l, v_t, and v_m in m/s), and Debye temperature (θ_D in K) of $SnTiO_3$ and $PbTiO_3$.

Compounds	v_l	v_t	v_m	θ_D
$PbTiO_3$	5896.668	4474.306	3685.152	464.275
$SnTiO_3$	6984.239	5387.918	4278.532	543.34

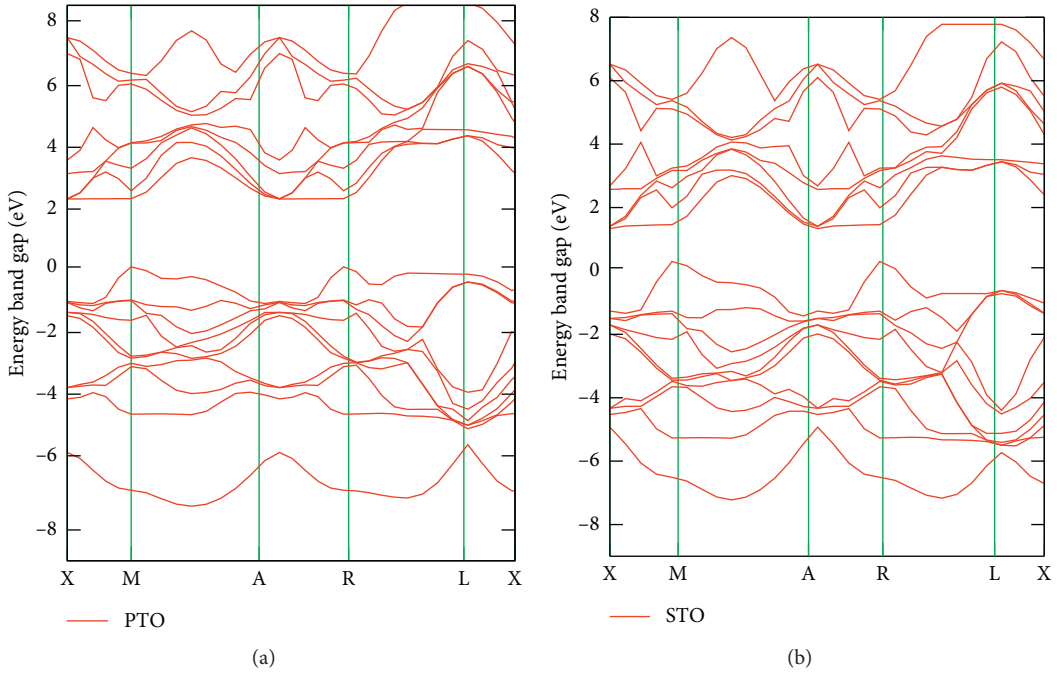

Figure 4: Electronic band structures of $PbTiO_3$ and $SnTiO_3$.

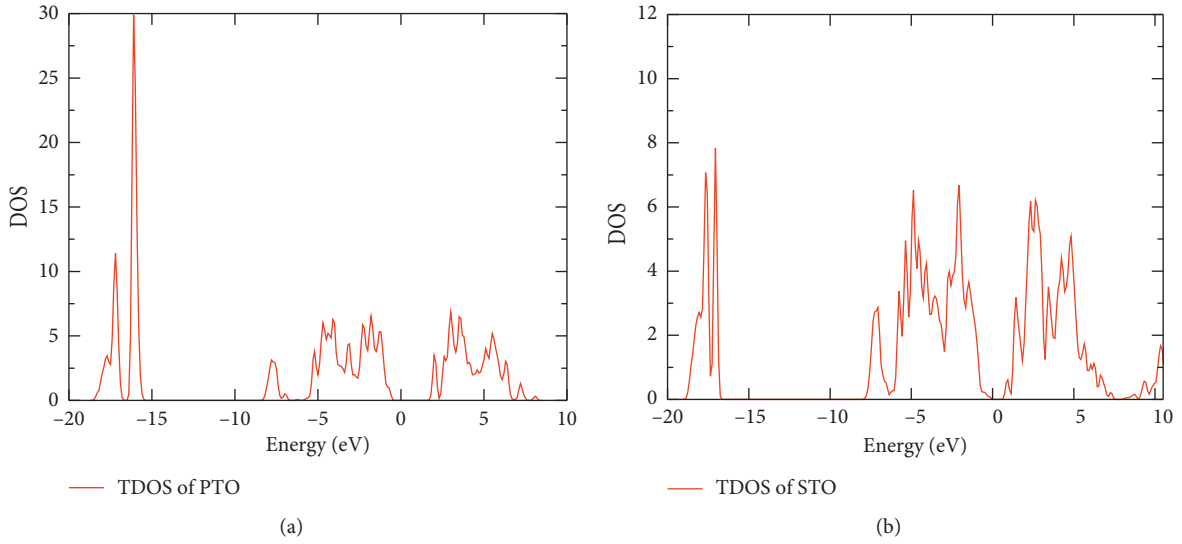

Figure 5: Total density of states of (a) $PbTiO_3$ and (b) $SnTiO_3$.

where the sum runs over occupied bands, k is parallel to the direction of polarization, and G is a reciprocal lattice vector in the same direction. The state u_{nk} is the lattice-periodical part of the Bloch wave function. The ionic part of polarization is a well-defined quantity from electromagnetic theory. Moreover, the electronic part of polarization cannot

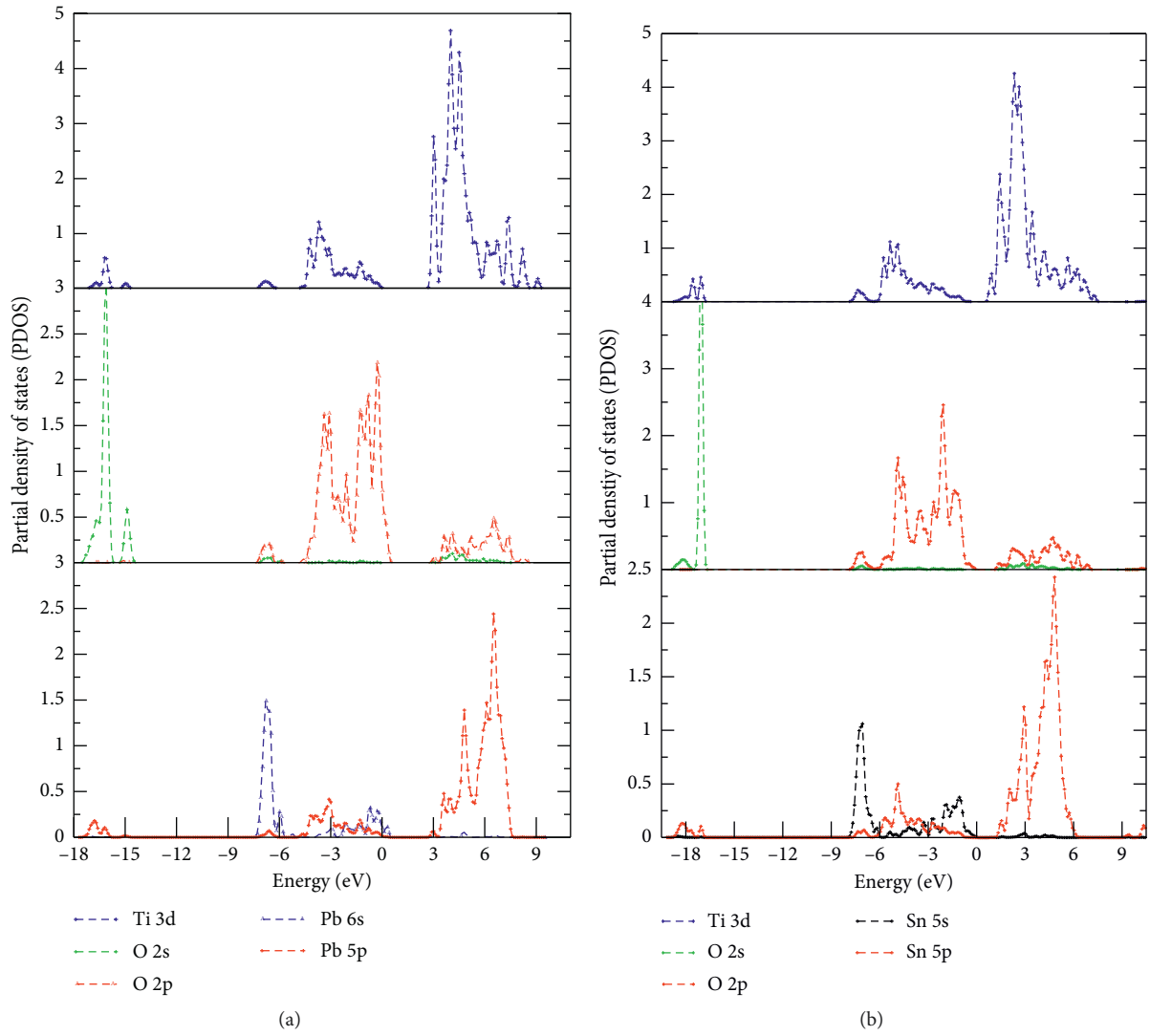

Figure 6: Partial density of states of (a) $PbTiO_3$ and (b) $SnTiO_3$.

be directly evaluated on the basis of localized contributions. The calculated spontaneous polarization at the equilibrium lattice constant by Berry's approach was determined to be 1.215 C/m^2 ($SnTiO_3$) and 0.9066 C/m^2 ($PbTiO_3$). The obtained values are in better agreement with the previous theoretical and experimental results.

4. Conclusions

In summary, we have carried out first principle calculations to investigate the structural, elastic, lattice dynamics, and electronic properties of $SnTiO_3$ and $PbTiO_3$. The ground-state parameters such as equilibrium lattice constant, bulk modulus, and its pressure derivatives are determined and relatively in good agreement with the available experimental results and previous theoretical data. The elastic constants, bulk, shear, and Young's modulus, Poisson's ratio, and anisotropy factor of both compounds are calculated and found in a better agreement with experimental and theoretical values. When the value of shear modulus increases, the material becomes stiffer. Thus, $PbTiO_3$ ($G = 84.3$) is stiffer than $SnTiO_3$ ($G = 81.9$). The quotient of bulk modulus to the shear modulus *(B/G)* is an indication of fracture in the system. Analyzing the ratio *B/G* is associated with ease of plastic deformation, and the high value indicates ductility. From this result, we conclude that both compounds are classified as ductile materials. The resistance of plastic deformation is proportional to the elastic shear modulus, while the fracture strength is proportional to the bulk modulus and the lattice constant. The elastic properties are closely related to the crystal structure and the nature of bonding among the ions within the compound. These factors can also determine the phonon spectrum and the Debye temperature. In general, the elastic constants are the important parameters to understand the mechanical properties and the phenomenon of superconductivity. The obtained Poisson's ratio of $PbTiO_3$ and $SnTiO_3$ are 0.26 and 0.28, respectively. This indicates that the interatomic forces are central. Moreover, the anisotropy factor suggests that both compounds exhibit comparatively small anisotropic elasticity in tetragonal

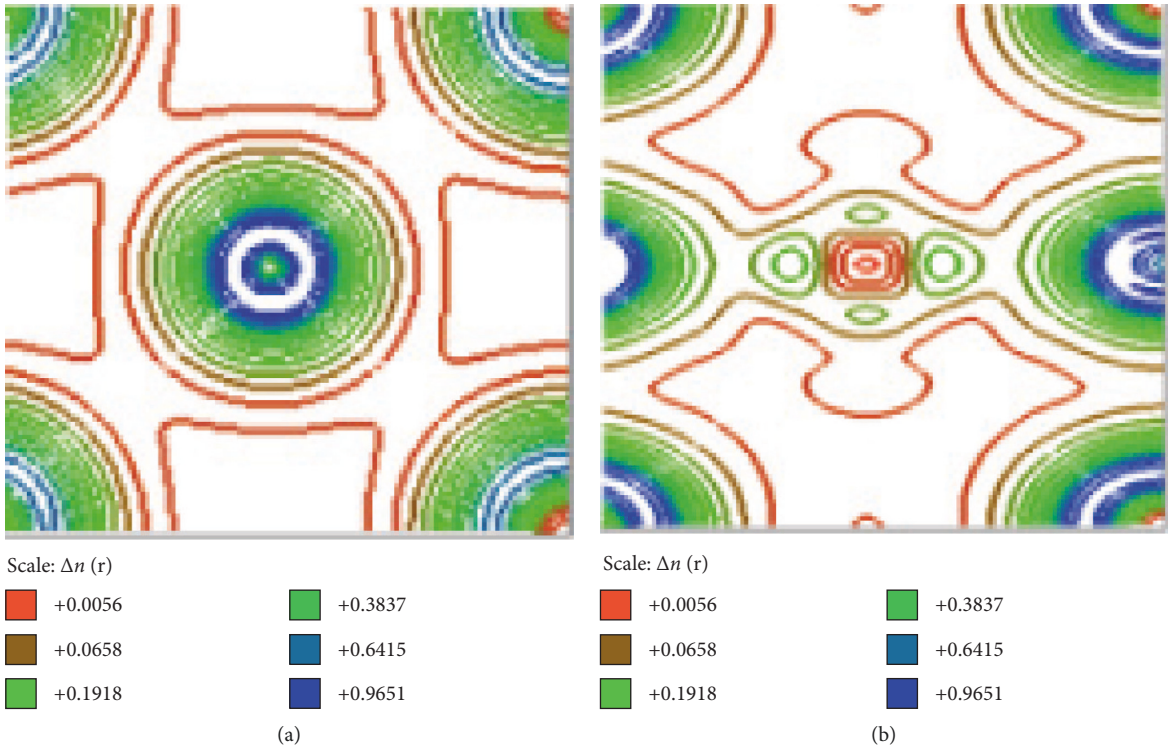

Figure 7: Electronic charge density in 100 and 110 plane of $PbTiO_3$ compound.

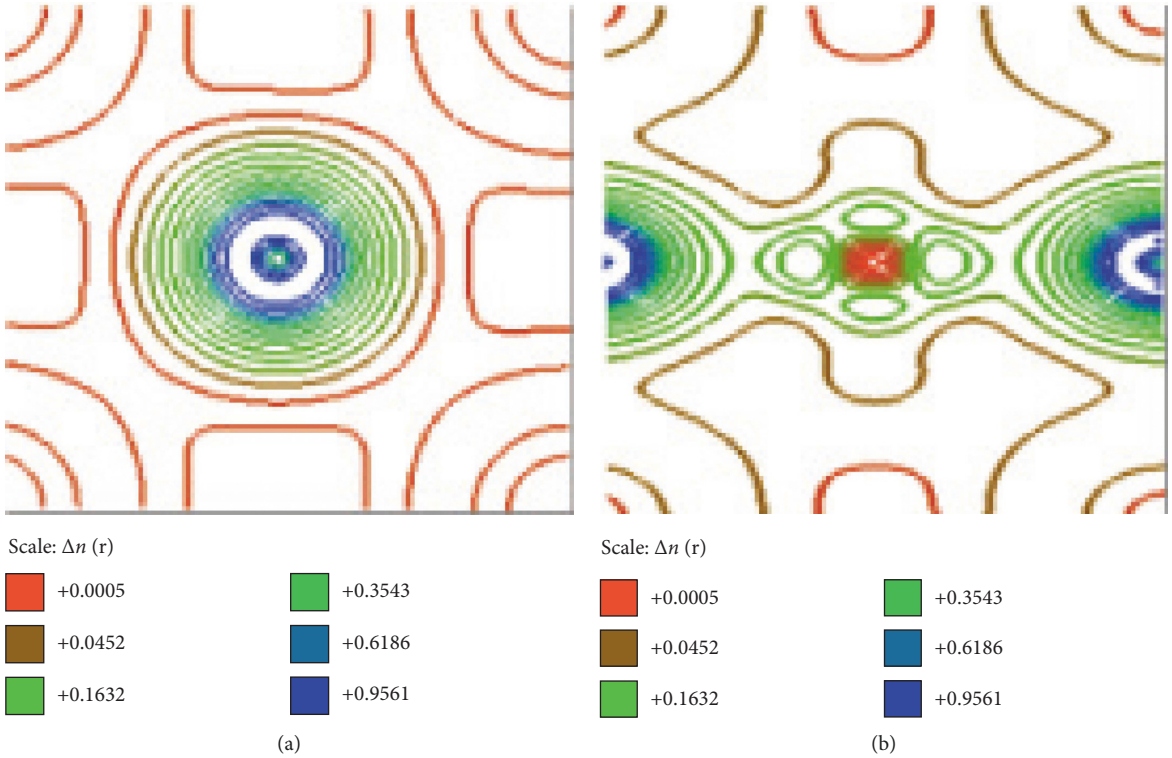

Figure 8: Electronic charge density in 100 and 110 plane of $SnTiO_3$ compound.

phase of materials. Furthermore, longitudinal and transverse sound velocity and Debye temperature have been investigated. The electronic properties of both compounds have indirect band gap value of 1.71 ($SnTiO_3$) and 2.21 ($PbTiO_3$). The obtained band gap is smaller than the experimental value as GGA fails to approximate the exact

Table 4: Born effective charge tensor of Pb, Sn, and Ti of $SnTiO_3$ and $PbTiO_3$ in the ferroelectric phase.

Z^* of Sn and Ti of $SnTiO_3$			Z^* of Pb and Ti of $PbTiO_3$		
Z^* Sn	Z^* Sn_{11}	4.21722	Z^* Pb	Z^* Pb_{11}	3.84594
	Z^* Sn_{22}	4.21722		Z^* Pb_{22}	3.84594
	Z^* Sn_{33}	4.04787		Z^* Pb_{33}	3.63015
Z^* Ti	Z^* Ti_{11}	7.57676	Z^* Ti	Z^* Ti_{11}	7.77463
	Z^* Ti_{22}	7.57676		Z^* Ti_{22}	7.77463
	Z^* Ti_{33}	6.70695		Z^* Ti_{33}	6.55227

Table 5: Born effective charge tensor of oxygen atoms of $SnTiO_3$ and $PbTiO_3$.

	Z^* of oxygen atoms of $SnTiO_3$	Z^* of oxygen atoms of $PbTiO_3$
O_1	$\begin{bmatrix} -2.780 & 0 & 0 \\ 0 & -2.780 & 0 \\ 0 & 0 & -5.350 \end{bmatrix}$	$\begin{bmatrix} -2.691 & 0 & 0 \\ 0 & -2.691 & 0 \\ 0 & 0 & -5.125 \end{bmatrix}$
O_2	$\begin{bmatrix} -2.461 & 0 & 0 \\ 0 & -6.140 & 0 \\ 0 & 0 & -2.515 \end{bmatrix}$	$\begin{bmatrix} -2.295 & 0 & 0 \\ 0 & -6.242 & 0 \\ 0 & 0 & -2.339 \end{bmatrix}$
O_3	$\begin{bmatrix} -6.140 & 0 & 0 \\ 0 & -2.461 & 0 \\ 0 & 0 & -2.515 \end{bmatrix}$	$\begin{bmatrix} -6.242 & 0 & 0 \\ 0 & -2.295 & 0 \\ 0 & 0 & -2.339 \end{bmatrix}$

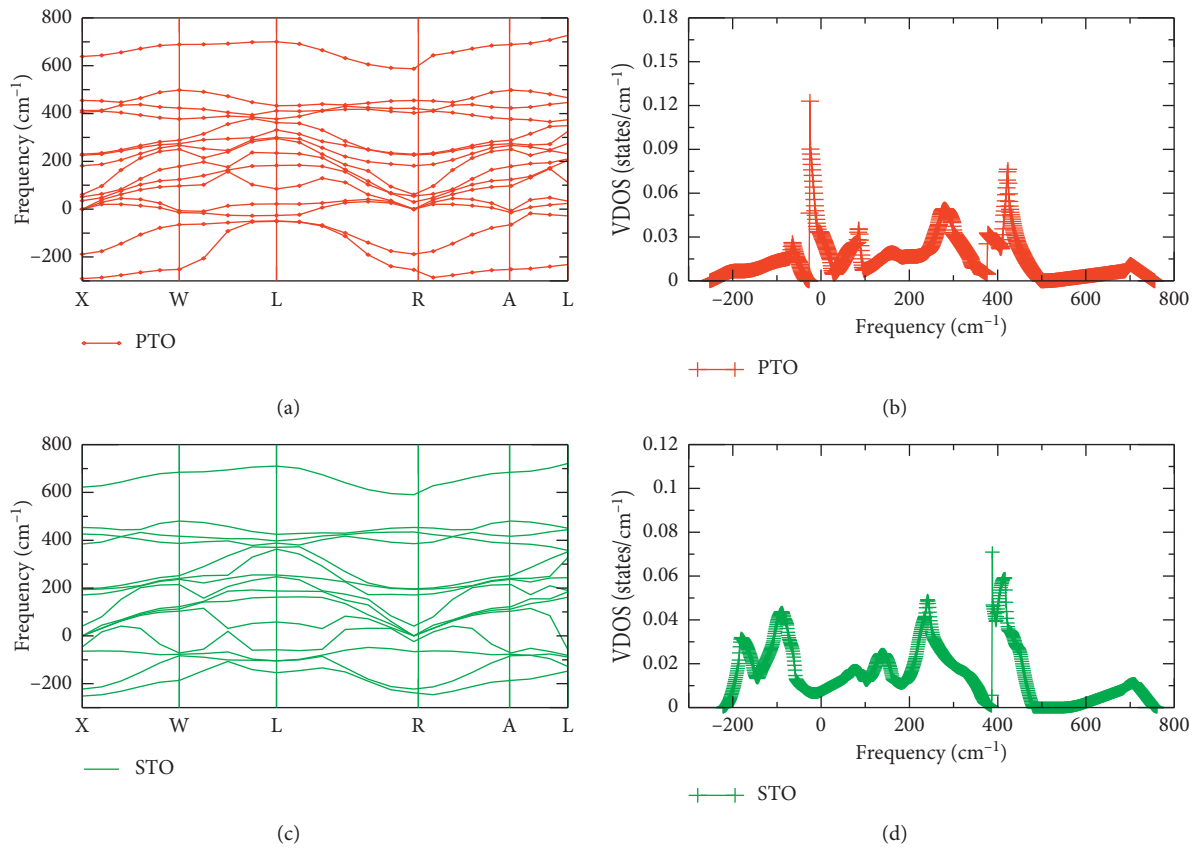

Figure 9: Phonon dispersion and vibrational density of states of $SnTiO_3$ and $PbTiO_3$.

exchange-correlation functional. The total density of state calculation shows that the top of the valance band of both compounds is dominated by O-2p states; however, the lower part of the conduction band by Ti-3d states. BEC, dielectric constant, phonon dispersion curve, and density of states are computed from DFPT using LDA. BEC values play a crucial

role in understanding the polar ground state and lattice dynamics of this perovskite material. The calculated BECs are larger compared to the nominal ionic charge. Using Berry phase approach, the spontaneous polarization was determined and its value is 1.215 C/m^2 ($SnTiO_3$) and 0.9066 C/m^2 ($PbTiO_3$). The large value of BEC of each atom in tetragonal phase of $PbTiO_3$ and $SnTiO_3$ compared to the nominal ionic charge reveals the importance of ions for the distortion of ferroelectricity. The obtained spontaneous polarization of $SnTiO_3$ shows high ferroelectric behavior compared to $PbTiO_3$. So, it can be a good candidate for application of ferroelectric materials.

Data Availability

All data relevant to this publication are included in the text and hence are available to everyone.

Conflicts of Interest

The authors declare that there are no conflicts of interest.

Acknowledgments

Shiferaw Gadisa expresses his thanks and appreciation to the Department of Physics, Wollega University, for its material support during this study.

References

[1] R. I. Eglitis, "Comparative first-principles calculations of $SrTiO_3$, $BaTiO_3$, $PbTiO_3$ and $CaTiO_3$ (001), (011) and (111) surfaces," *Ferroelectrics*, vol. 483, no. 1, pp. 53–67, 2015.

[2] O. Auciello, J. F. Scott, and R. Ramesh, "The physics of ferroelectric memories," *Physics Today*, vol. 51, no. 7, pp. 22–27, 1998.

[3] R. J. Nelmes and W. F. Kuhs, "The crystal structure of tetragonal $PbTiO_3$ at room temperature and at 700 K," *Solid State Communications*, vol. 54, no. 8, pp. 721–723, 1985.

[4] R. E. Cohen and H. Krakauer, "Electronic structure studies of the differences in ferroelectric behavior of $BaTiO_3$ and $PbTiO_3$," *Ferroelectrics*, vol. 136, no. 1, pp. 65–83, 1992.

[5] S. Piskunov, E. Heifets, R. I. Eglitis, and G. Borstel, "Bulk properties and electronic structure of $SrTiO_3$, $BaTiO_3$, $PbTiO_3$ perovskites: an ab initio HF/DFT study," *Computational Materials Science*, vol. 29, no. 2, pp. 165–178, 2004.

[6] L. Wang, P. Yuan, F. Wang et al., "First-principles study of tetragonal $PbTiO_3$: phonon and thermal expansion," *Materials Research Bulletin*, vol. 49, pp. 509–513, 2014.

[7] F. O. Ongondo, I. D. Williams, and T. J. Cherrett, "How are WEEE doing? A global review of the management of electrical and electronic wastes," *Waste Management*, vol. 31, no. 4, pp. 714–730, 2011.

[8] M. F. M. Taib, M. K. Yaakob, M. S. A. Rasiman, F. W. Badrudin, O. H. Hassan, and M. Z. A. Yahya, "Comparative study of cubic Pm3m between $SnZrO_3$ and $PbZrO_3$ by first principles calculation," in *Proceedings of the Humanities, Science and Engineering (CHUSER)*, pp. 713–718, IEEE, Kota Kinabalu, Malaysia, December 2012.

[9] M. F. M. Taib, M. K. Yaakob, F. W. Badrudin, T. I. T. Kudin, O. H. Hassan, and M. Z. A. Yahya, "First principles calculation of tetragonal (P4 mm) Pb-free ferroelectric oxide of $SnTiO_3$," *Ferroelectrics*, vol. 459, no. 1, pp. 134–142, 2014.

[10] M. F. M. Taib, M. K. Yaakob, F. W. Badrudin et al., "First-principles comparative study of the electronic and optical properties of tetragonal (P4mm) $ATiO_3$ (A = Pb, Sn, Ge)," *Integrated Ferroelectrics*, vol. 155, no. 1, pp. 23–32, 2014.

[11] R. I. Eglitis and A. I. Popov, "Systematic trends in (0 0 1) surface ab initio calculations of ABO_3 perovskites," *Journal of Saudi Chemical Society*, vol. 22, no. 4, pp. 459–468, 2018.

[12] R. I. Eglitis, "Ab initio hybrid DFT calculations of $BaTiO_3$, $PbTiO_3$, $SrZrO_3$ and $PbZrO_3$ (111) surfaces," *Applied Surface Science*, vol. 358, pp. 556–562, 2015.

[13] J. P. Perdew, K. Burke, and M. Ernzerhof, "Generalized gradient approximation made simple," *Physical Review Letters*, vol. 77, no. 18, pp. 3865–3868, 1996.

[14] H. J. Monkhorst and J. D. Pack, "Special points for Brillouin-zone integrations," *Physical Review B*, vol. 13, no. 12, pp. 5188–5192, 1976.

[15] V. A. Chaudhari and G. K. Bichile, "Synthesis, structural, and electrical properties of pure $PbTiO_3$ ferroelectric ceramics," *Smart Materials Research*, vol. 2013, Article ID 147524, 9 pages, 2013.

[16] J. Long, L. Yang, and X. Wei, "Lattice, elastic properties and Debye temperatures of $ATiO_3$ (A=Ba, Ca, Pb, Sr) from first-principles," *Journal of Alloys and Compounds*, vol. 549, pp. 336–340, 2013.

[17] F. D. Murnaghan, "The compressibility of media under extreme pressures," *Proceedings of the National Academy of Sciences*, vol. 30, no. 9, pp. 244–247, 1944.

[18] J. H. Weiner, *Statistical Mechanics of Elasticity*, Courier Corporation, Chelmsford, MA, USA, 2012.

[19] P. Giannozzi, O. Andreussi, T. Brumme et al., "Advanced capabilities for materials modelling with Quantum ESPRESSO," *Journal of Physics: Condensed Matter*, vol. 29, no. 46, Article ID 465901, 2017.

[20] A. Hachemi, H. Hachemi, A. Ferhat-Hamida, and L. Louail, "Elasticity of $SrTiO_3$ perovskite under high pressure in cubic, tetragonal and orthorhombic phases," *Physica Scripta*, vol. 82, no. 2, Article ID 025602, 2010.

[21] Z. Li, M. Grimsditch, C. M. Foster, and S.-K. Chan, "Dielectric and elastic properties of ferroelectric materials at elevated temperature," *Journal of Physics and Chemistry of Solids*, vol. 57, no. 10, pp. 1433–1438, 1996.

[22] W. Voigt, *Lehrbuch der Kristallphysik (mit Ausschluss der Kristalloptik)*, B. G. Teubner, Berlin, Germany, 1910.

[23] A. Reuss, "Berechnung der fließgrenze von mischkristallen auf grund der plastizitätsbedingung für einkristalle," *ZAMM—Zeitschrift für Angewandte Mathematik und Mechanik*, vol. 9, no. 1, pp. 49–58, 1929.

[24] R. Hill, "The elastic behaviour of a crystalline aggregate," *Proceedings of the Physical Society, Section A*, vol. 65, no. 5, pp. 349–354, 1952.

[25] S. F. Pugh, "XCII. Relations between the elastic moduli and the plastic properties of polycrystalline pure metals," *The London, Edinburgh, and Dublin Philosophical Magazine and Journal of Science*, vol. 45, no. 367, pp. 823–843, 1954.

[26] S. I. Ranganathan and M. Ostoja-Starzewski, "Universal elastic anisotropy index," *Physical Review Letters*, vol. 101, no. 5, Article ID 055504, 2008.

[27] P. Ravindran, L. Fast, P. A. Korzhavyi, B. Johansson, J. Wills, and O. Eriksson, "Density functional theory for calculation of elastic properties of orthorhombic crystals: application to TiSi2," *Journal of Applied Physics*, vol. 84, no. 9, pp. 4891–4904, 1998.

[28] P. Vajeeston, P. Ravindran, and H. Fjellvåg, "Prediction of structural, lattice dynamical, and mechanical properties of CaB_2," *RSC Advances*, vol. 2, no. 31, pp. 11687–11694, 2012.

[29] X. Li, C. Xia, M. Wang, Y. Wu, and D. Chen, "First-principles investigation of structural, electronic and elastic properties of HfX (X = Os, Ir and Pt) compounds," *Metals*, vol. 7, no. 8, p. 317, 2017.

[30] S. F. Matar, I. Baraille, and M. A. Subramanian, "First principles studies of $SnTiO_3$ perovskite as potential environmentally benign ferroelectric material," *Chemical Physics*, vol. 355, no. 1, pp. 43–49, 2009.

[31] Y. Konishi, O. Michio, Y. Yonezawa et al., "Possible ferroelectricity in $SnTiO_3$ by first-principles calculations," *MRS Online Proceedings Library Archive*, vol. 748, 2002.

[32] H. O. Yadav, "Optical and electrical properties of sol-gel derived thin films of $PbTiO_3$," *Ceramics International*, vol. 30, no. 7, pp. 1493–1498, 2004.

[33] R. E. Cohen, "Origin of ferroelectricity in perovskite oxides," *Nature*, vol. 358, no. 6382, p. 136, 1992.

[34] X. Gonze and C. Lee, "Dynamical matrices, Born effective charges, dielectric permittivity tensors, and interatomic force constants from density-functional perturbation theory," *Physical Review B*, vol. 55, Article ID 10355, 1997.

[35] M. Kamruzzaman, M. A. Helal, I. E. Ara, A. K. M. F. Ul Islam, and M. M. Rahaman, "A comparative study based on the first principles calculations of $ATiO_3$ (A = Ba, Ca, Pb and Sr) perovskite structure," *Indian Journal of Physics*, vol. 90, no. 10, pp. 1105–1113, 2016.